Grain growth in strontium titanate in electric fields: the impact of space charge on the grain boundary mobility

Wolfgang Rheinheimer[*,1], Jana P. Parras[3], Jan-Helmut Preusker[2], Roger A. De Souza[3] and Michael J. Hoffmann[2]

[*] Corresponding author, rheinheimer@purdue.edu

[1] Purdue University, Materials Engineering, 701 West Stadium Ave, 47907 West Lafayette, Indiana, USA

[2] Karlsruhe Institute of Technology (KIT), Institute of Applied Materials – Ceramic Materials and Technologies (IAM-KWT), Haid-und-Neu-Str. 7, 76131 Karlsruhe, Germany

[3] RWTH Aachen University, Institute of Physical Chemistry, Landoltweg 2, 52074 Aachen, Germany

Abstract

The present study investigates grain growth in strontium titanate in an electric field. The experimental setup used current blocking electrodes to prevent Joule heating. The seeded polycrystal technique was chosen as it provides a sensitive and controlled setup to evaluate the impact of different parameters on grain growth due to the well-defined driving force for grain growth. The results show faster grain growth and, thus, higher grain boundary mobility on the negative electrode.

It is argued that a defect redistribution seems to be caused by the electric field resulting in a higher oxygen vacancy concentration at the negative electrode. A thermodynamic calculation of the grain boundary potential and space charge shows that for a high oxygen vacancy concentration less space charge and less accumulation of charged defects to the boundary occurs. Therefore, at the negative electrode, a higher oxygen vacancy concentration results in less space charge and less accumulation of charged defects. For grain boundary migration, less defect accumulation might result in less diffusion of segregated defects, so that at the negative electrode faster grain growth is expected as found in the experiments.

Key words

grain growth, grain boundaries, segregation, Field Assisted Sintering Technology (FAST), defects, space charge

1. Introduction

In the past fifteen years, considerable effort was put into investigating the effect of electric field during sintering, e.g. with respect to Spark Plasma Sintering (SPS), where electric currents are used to directly heat a material enclosed in a graphite die while simultaneously a mechanical pressure is applied [1-5]. Since 2010, another field assisted sintering process named flash sintering attracted attention [6]. In this process, an electric power dissipation in a preheated ceramic green body is used to induce a thermal runaway with extremely fast heating rates so that sintering within seconds can be achieved [7-9].

However, revealing the underlying mechanisms in field assisted sintering (SPS and flash sintering) is very challenging, because the electric power dissipation leads to Joule heating in the material such that the true temperatures are hard to access. The fast heating rates add to the poor controllability of the sintering process. Accordingly, there still is a vivid debate particularly on the mechanism for flash sintering. Some authors argue that the electric field impacts the point defect chemistry yielding a drastically increased vacancy concentration, which then increases the diffusion coefficients and eases densification [10, 11]. Others argue that the high current density in the sintering neck area during field assisted sintering locally causes very high temperatures, so that melting occurs in the sintering neck area thereby yielding very quick densification [12, 13]. Finally, some studies indicate that the fast densification during flash sintering is solely caused by Joule heating of the entire green body and the extremely fast heating rates [14-16].

While the complexity of field assisted sintering prevents careful investigation of underlying mechanisms, several different model experiments allow better controllability of the experimental parameters (e.g. fast heating without electric power dissipation [15], slow heating with electric power dissipation [16], sintering with electric fields but without power dissipation [17] or grain growth with electric power dissipation [18, 19]). The most simplified case is observing grain growth (i.e. no shrinkage) in electric field, but without electric power dissipation (i.e. with blocking electrodes). This experiment was conducted in a previous study on strontium titanate [20], a material for which vast information is available on microstructure evolution in the absence of electric field [21-23], point defect chemistry [24] and interfacial properties [25-27]. In this experiment, the seeded polycrystal technique was used. This technique uses a singlecrystalline seed diffusion bonded to a polycrystalline matrix to establish a well-defined driving force for grain growth [28-30]. The electric field was found to induce a gradient of the growth rate of the single crystal between the two electrodes with grain growth being faster on the negative electrode. A point defect redistribution was presumed yielding a higher oxygen vacancy concentration on the negative electrode.

The present paper adds more growth data and some information on the diffusion kinetics to detail the defect distribution profile in electric fields. A thermodynamic calculation of the space

charge of strontium titanate reveals that the change in grain growth rate by the oxygen partial pressure seems to be due to a change in grain boundary potential and defect accumulation: for high $p(O_2)$, strong space charge and defect accumulation where found while for low $p(O_2)$, almost no space charge and defect accumulation occur. Since the segregated species (both intrinsic defects as Sr vacancies and extrinsic defects as impurities) diffuse along with the grain boundary migration, a diffusional drag seems to exist for high oxygen partial pressure, but not for low oxygen partial pressure.

2. Experimental Procedure

2.1. ***The seeded polycrystal technique in electric field***

Stoichiometric undoped strontium titanate powder was prepared by the mixed oxide/carbonate route using high purity raw materials ($SrCO_3$ and TiO_2, both 99.9+%, Sigma Aldrich Chemie GmbH, Taufkirchen, Germany). Dense (99.5 ± 0.2 %) polycrystalline samples were obtained by conventional sintering at 1425 °C for 1 h in oxygen in a tube furnace (Carbolite Gero, Neuhausen, Germany). More details of the powder synthesis can be found elsewhere [21]. Samples were cut into discs of a thickness of 1 mm and polished (diamond slurry, 0.25 µm) and then scratched with a polishing disc (30 µm diamonds). Theses scratches are needed to create pore channels during diffusion bonding of the seeded polycrystals so that the original position of the interface is marked (Figure 1c [20, 28, 29]).

To demonstrate the impact of an electric field on grain growth, the seeded polycrystal technique was used. In this method, a singlecrystalline seed is diffusion bonded to a polycrystalline matrix. In a subsequent annealing, the single crystal grows into the polycrystal. The driving force for this growth is provided by the capillarity of the grain boundaries in the polycrystal. To fabricate suitable samples, a single crystalline disc (chemical-mechanical polished, impurity content: <10 ppm Si, <2 ppm Ba, <1 ppm Ca, SurfaceNet GmbH, Rheine, Germany) with a thickness of 1 mm was placed between two polycrystalline discs. Joining was achieved by a diffusion bonding process in a mechanical load frame with attached furnace (1430 °C, 20 min in air, 1 MPa, Amsler, Neftenbach, Switzerland). To prevent a chemical reaction or bonding of the sample to the alumina rods of the load frame, a thin layer of coarse-grained zirconia powder was placed between the sample and the alumina supports. Further details of this procedure are published elsewhere [20, 28, 29].

For applying an electric field along the interface of the single crystalline seeds during grain growth, the seeded polycrystals were again cut perpendicular to the single crystal in slices of a thickness of 2 mm. To avoid joule heating by a current flowing through the sample, samples were placed between two high purity alumina plates (thickness of 1 mm) as shown in Figure 1a. To prevent any reaction of strontium titanate with the alumina, a very thin layer (<0.1 mm)

of coarse zirconia powder was spread in the contact area to prevent a direct contact. No influence or reaction of the zirconia on the strontium titanate was found.

On top of both alumina plates platinum sheets were used as electrodes. The electrodes were welded to platinum wires which were guided outside the furnace to a voltage source (XG 600-2.8, AMETEK, San Diego, USA). The electric fields over the entire setup including alumina insulators were 25 V/mm or 50 V/mm. Note that the field in the sample is smaller, because in the alumina insulator plates with relatively low dielectric constant some electric field is lost [20]. The true fields in the strontium titanate sample where estimated to be about 50% of the overall electric field. Voltage and current were measured and logged (Type GL200A, Graphtec Corp., Yokohama, Japan). During all experiments, the current was below the detection limit due to the insulating alumina plates. All grain growth experiments were performed in a batch furnace between 1425 °C and 1550 °C in air (Carbolite Gero, Neuhausen, Germany).

The mean grain radius of the polycrystalline matrix was obtained by the line intersection method on SEM micrographs. To capture the microstructural gradient along the electric field, on each sample three different positions were observed (close to both electrodes and in the center of the sample). Each measurement bases on typically 200 grains (min. 120). The growth of the single crystalline seed was measured by assembling 5-10 SEM images to one image across the entire interface (Figure 1b). In these assembled images the growth length of the seed was detected and plotted with respect to its position in the sample (thin line in Figure 2 and Figure 3). Additionally the data was fitted with a polynomial of second degree to highlight the trend of the growth length (thick line in in Figure 2 and Figure 3).

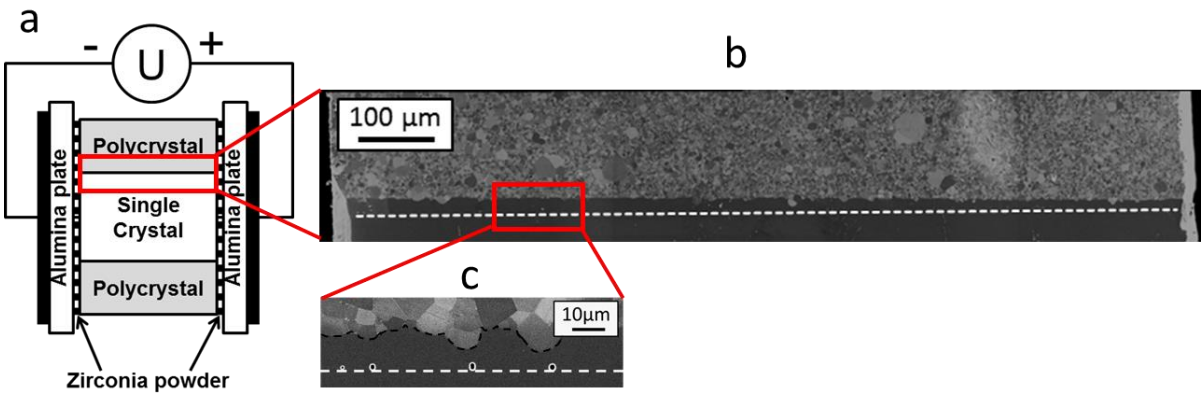

Figure 1 experimental setup used in the present experiments (a). The sample geometry corresponds to the seeded polycrystal technique. An electric field was applied along the interface of the single crystal with platinum sheets as electrodes. Alumina plates where used to block electric and ionic currents at high temperatures. A thin layer of zirconia powder prevented a chemical reaction between the alumina and the strontium titanate. A typical growth front of the single crystal across the sample is shown in b and c in two magnifications. The white broken line represents the initial position of the growth front. At higher magnification, small pores are visible that originate in the diffusion bonding process and mark the initial position of the growth front (c).

2.2. ***Calculation of the space charge layers with respect to oxygen partial pressure***

Space-charge layers are regions of altered bulk defect concentrations caused by the presence of an extended defect, such as an interface. Hence, in order to calculate the potential at a grain boundary, one has to specify the point-defect concentrations in the electroneutral bulk phase and one has to link the interfacial defect chemistry to that of the bulk phase [27].

Point-defect concentrations were calculated by means of the standard defect chemical model for acceptor-doped $SrTiO_3$ [24, 31-33], a model that includes electron-hole generation across the band gap, reduction of the oxide and SrO partial Schottky disorder. Values for the equilibrium constants of these reactions were taken from Moos and Härdtl [24]. The model yields, for given acceptor-dopant concentration, temperature and oxygen partial pressure, the concentrations of oxygen vacancies, electron holes, strontium vacancies and electrons.

The link to the interfacial defect chemistry consists of specifying the thermodynamic driving energies for point defect redistribution from the bulk to the interface, or vice versa [27, 34]. In the present case, we assume a single thermodynamic driving energy, namely that the standard chemical potential of oxygen vacancies is lower at the interface than in the bulk phase ($\Delta\mu_V^{\ominus} < 0$). As a consequence, oxygen vacancies segregate to the interface, charging it positively, and thus generating negative space charge zones depleted of vacancies. All other point defects are assumed to be mobile and to redistribute based on the electric field set up by the

redistribution of the oxygen vacancies. The equilibrium situation corresponds to electrochemical potential of each defect being constant throughout the system. The standard expression for the electrochemical potential of a point defect building unit is used [27]:

$$\tilde{\mu} = \mu^{\ominus} + k_B T \left[\frac{c(x)}{N - c(x)}\right] + ze\phi(x) \qquad (1)$$

The physical model that we employed is a one-dimensional model, in which a grain-boundary of finite width is sandwiched between two semi-infinite blocks of the bulk phase. Poisson's equation is solved for the entire simulation cell,

$$\epsilon_0 \epsilon_r \frac{d^2\phi(x)}{dx^2} = -\rho, \qquad (2)$$

with electrical potential ϕ, the vacuum and relative permittivity ϵ_r and ϵ_r and the space charge density ρ. Finite-element-method calculations are used to solve Eq. (2) numerically, with boundary condition $\phi(\infty) = 0$. The space-charge density is given by

$$\rho(x) = -e\, c_{\mathrm{dop}}(x) + 2\, e\, c_{\mathrm{v_O}}(x) + e\, c_{\mathrm{h}}(x) - 2\, e\, c_{\mathrm{v_{Sr}}}(x) - e\, c_{\mathrm{e}}(\mathrm{x}) \qquad (3)$$

The concentration profiles *c*(x) are obtained from Eq. (1).

3. Results and Discussion

3.1. *Grain growth in electric field perpendicular to the growth direction*

Figure 2 shows the growth of the single crystalline seeds into the polycrystalline matrix at 1425 °C after 10 h (a, c) and 20 h (b, d) for 25 V/mm (a, b) and 50 V/mm (c, d). Each plot gives the position of the growth front of both interfaces of the single crystalline seed with respect to the position in the sample. The negative (positive) electrode was on the left (right) side. The mean grain size is indicated by black squares for three sample positions. In the case of Figure 2b, one interface of the sample broke during the experiment so that only one curve is shown in the graph. In all other cases, both interfaces where observed and show good agreement with each other.

In general, the mean grain size is analogue to the growth of the single crystals as is to be expected from mean-field modelling for the seeded polycrystal technique [28]. However, for microstructures with weak gradients, the gradient in the mean grain size is very small. Accordingly, the growth front of the single crystal is more significant for our analysis as it gives continuous data with good statistics over the entire sample.

After 10 h at 1425 °C with 25 V/mm, the growth of the single crystal does not depend on the position in the sample and the growth front is almost horizontal (Figure 2a). The scattering in the data is because of the grain size in the polycrystal as evident in Figure 1b and c. A more detailed discussion of microstructures and scattering can be found in the literature [20]. However, the trendline (thick line in Figure 2a) and mean grain sizes show that no gradient in the microstructure is visible across the sample. At 50 V/mm a slight gradient appears.

However, for longer heating times in Figure 2b and d show that the gradient in the microstructure increases with time and becomes evident even at 25 V/mm.

It should be noted that, in principle, a gradient in the growth length can only occur if the single crystal shows enough growth during the experiment: a non-growing single crystal will not show different growth rates no matter what the electric field is. The growth distance in Figure 2 is 5µm and more, which is significant growth during the experiment with electric field [28]. Accordingly, the presence (or absence) of gradients at 1425 °C can be attributed to the impact (or irrelevance) of the electric field.

At 1550 °C, even the shortest feasible heating time of 6 min resulted in strong gradients in the microstructure as shown in Figure 3a and c. For longer heating times, these gradients become more pronounced, but do not change in general. Again, the mean grain size correlates well with the growth of the single crystals.

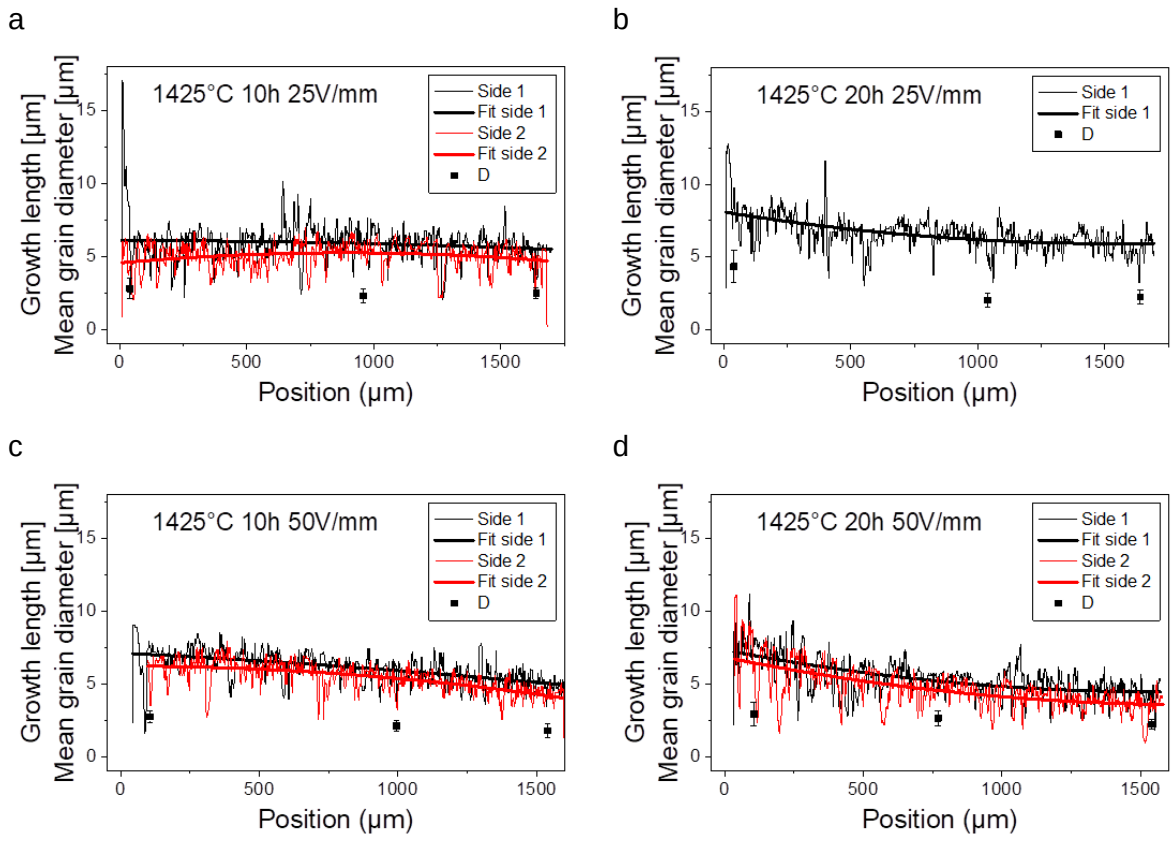

Figure 2: Growth length of the single crystals in electric field at 1425 °C after 10 h (a, c) and 20 h (b, d). The negative (positive) electrode was on the left (right) side. For a and b, the overall electric field was 25 V/mm (50 V/mm for c and d). In one case (b), parts of the sample fractured during preparation, so that only one curve could be obtained.

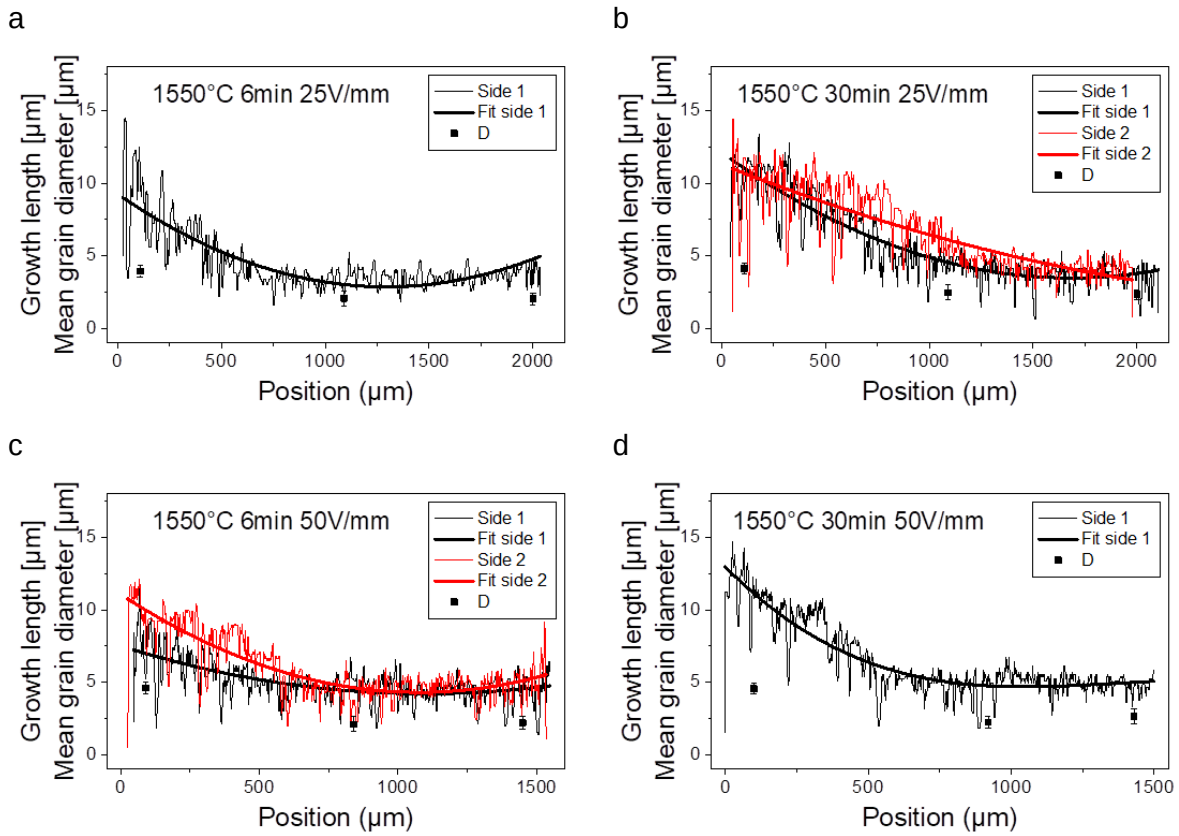

Figure 3: Growth length of the single crystals in electric field at 1550 °C after 6 min (a, c) and 30 min (b, d). The negative (positive) electrode was on the left (right) side. For a and b, the overall electric field was 25 V/mm (50 V/mm for c and d). In two cases (a, d), parts of the sample fractured during preparation, so that only one curve could be obtained.

3.2. ***Defect redistribution by the electric field***

In our previous study, we suggested that the gradients in the microstructure result of electromigration: in the electric field, positive (negative) point defects migrate towards the negative (positive) electrode [20]. As the experimental setup included current blocking electrodes, this migration builds up a polarization and an internal electric field with opposite direction of the external electric field. In general, this migration will come to an end, if the electrochemical potential of the respective defects is constant across the sample. Note that due to the blocking electrodes, the steady-state does not involve significant ion or electron fluxes. Besides of the kinetics (see section 3.4), this equilibrium defect concentration profile in electric field across the sample is of interest.

The exact shape of the equilibrium distribution is not easy to find. For strontium titanate the relevant point defect species are oxygen vacancies, strontium vacancies, acceptors, electrons and holes. As will be discussed later, it seems that the diffusion of acceptors and metal vacancies is too slow to play a significant role in the long range diffusion as needed for the defect redistribution by the electric field across the entire sample [35, 36]. Accordingly, we

assume that only electrons, holes and oxygen vacancies are redistributed. Here, we ignore the distribution of electrons and holes as they do not contribute to the grain boundary mobility.

In the literature, several detailed studies investigated the resistance degradation mechanism in acceptor doped perovskites [37-41]. As these studies observe a defect redistribution in electric fields in a very similar way to the present experiment, therein established point defect modelling [41] can be used to at least qualitatively estimate the defect concentration profile. As Figure 4 sketches, there are two possible equilibrium profiles. If the bulk defect chemistry remains unchanged for all positions of the sample, the equilibrium profile in electric field will have the shape of the red curve in Figure 4. However, if the local defect concentration at the negative electrode becomes too high, saturation effects might occur (blue curve in Figure 4). This saturation could result e.g. from interaction between the oxygen vacancies, that are no longer in a dilute concentration. Another possibility is the phase stability of the perovskite phase: for too high vacancy concentrations, the perovskite lattice will become unstable and decompose. However, with SEM and XRD, we found no evidence for a phase decomposition. Additionally, a saturation of the defect concentration should be visible in the shape of the growth front of the single crystal if a direct link between the local point defect concentration and the grain growth concentration exists as discussed in section 3.3. However, Figure 2 and Figure 3 do not show a correlation to the blue curve in Figure 4, but to the red curve. Accordingly, there is no evidence for a saturation of the oxygen vacancy concentration at the negative electrode and we assume the red curve to represent the equilibrium oxygen vacancy concentration in electric field.

While the exact distribution of the point defects during the experiment is not clear yet, it seems to be reasonable to argue that the point defect concentration shows a gradient between the electrodes with the maximum of the oxygen vacancy concentration at the negative electrode. From grain growth experiments in the absence of electric field it is known that grain growth is faster in reducing atmosphere (i.e. with a higher oxygen vacancy concentration [30]). Accordingly, faster growth at the negative electrodes in electric field as observed in Figure 2 and Figure 3 can be attributed to the local increase of the oxygen vacancy concentration.

So far, this argumentation bases only on the correlation between grain growth in the absence of electric fields, but with a change of the oxygen partial pressure with grain growth in electric field. In both cases, faster grain growth (i.e. a higher grain boundary mobility) occurs if the oxygen vacancy concentration is (or is supposed to be) high.

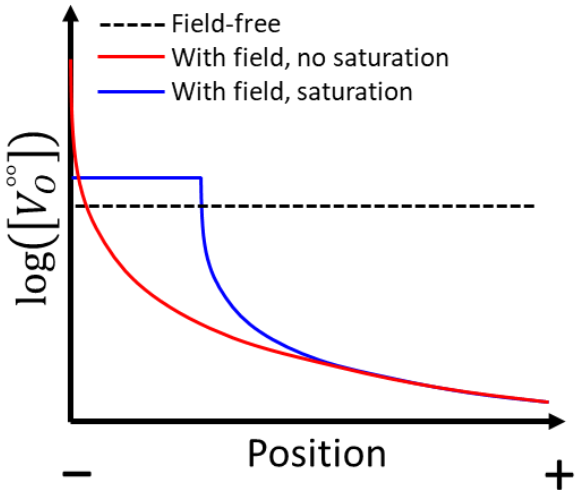

Figure 4: Sketch of the oxygen vacancy distribution across the sample without electric field (broken line), with electric field assuming no saturation of the oxygen vacancy concentration (red) and assuming a saturation concentration (blue line). The shape of the curves was taken from Wang et al. [41].

3.3. ***Relationship between defects, space charge and grain boundary mobility***

Following the previous paragraph, the correlation of grain growth in electric field with field-free grain growth with different oxygen partial pressure suggests a dependence of the grain boundary mobility of the point defect concentration. A possible mechanism for this relationship bases on space charge and its dependence on the oxygen partial pressure.

Strontium titanate is well-known to have a positive grain boundary potential and an adjacent negative space charge [27, 42, 43]. The space charge represents layers at the grain boundary with a change in the point defect concentration. Following the procedures from section 2.2, the space charge layer of strontium titanate was calculated for different oxygen partial pressures (10^{-20} – 1 bar). Figure 5a shows the calculated oxygen partial pressure dependent grain boundary potential of strontium titanate at 1400 °C. For high oxygen partial pressure, a high grain boundary potential was observed. Lowering the oxygen partial pressure from 1 bar will first result in a minor increase, but then a drastic decrease of the grain boundary potential down to almost 0 V at $p(O_2) = 10^{-20}$ bar. The resulting space charge profiles are shown in Figure 5b. The decreasing grain boundary potential from Figure 5a becomes evident again. In addition, the thickness of the space charge layer decreases with decreasing $p(O_2)$, because the total number of charged defects increases [24, 27]. As evident in Figure 5b, the space charge layer (i.e. potential height and layer thickness) becomes much weaker in lower oxygen partial pressure.

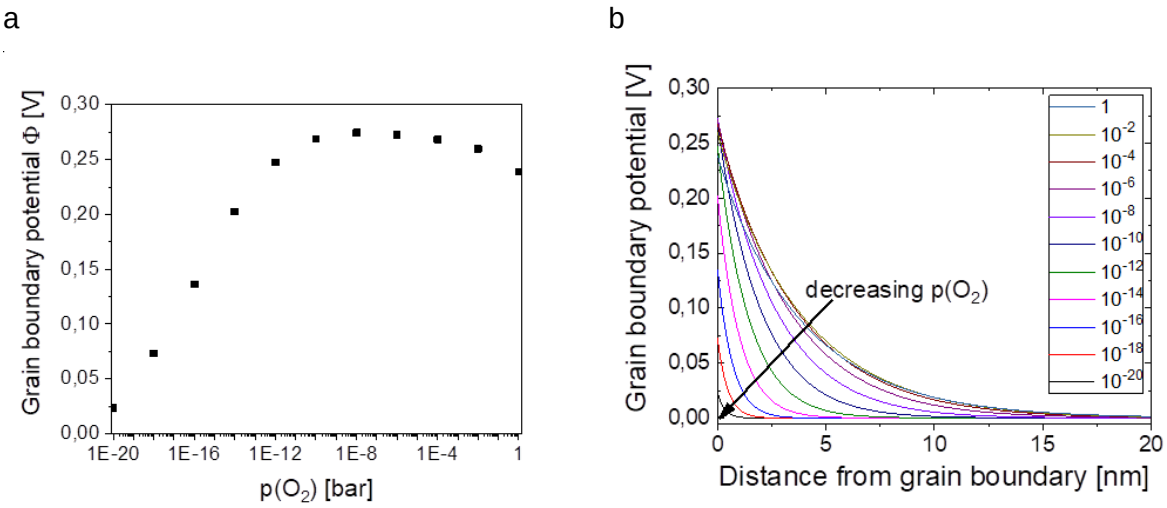

Figure 5 Calculated grain boundary potential at 1400 °C with respect to oxygen partial pressure (a) and the resulting potential distribution in the space charge layer (b).

Based on the potential distribution in Figure 5, the concentration profiles of all relevant defects (oxygen vacancies, strontium vacancies, acceptors, electrons and holes) in the space charge layer were calculated. Figure 6 shows the concentration profiles for a relatively high oxygen partial pressure of 10^{-4} bar (a) and for a relatively low oxygen partial pressure of 10^{-18} bar (b). For 10^{-4} bar, strontium vacancies, acceptors and electrons clearly accumulate at the grain boundary, while oxygen vacancies and holes are depleted. For 10^{-18} bar, two changes become evident. First, the bulk concentration of strontium vacancies and holes drops by more than one order of magnitude, while the bulk concentration of oxygen vacancies and electrons increases similarly. This is to be expected from the bulk defect chemistry of strontium titanate [24]. Second, the accumulation (depletion) of defects is only very minor: bulk and space charge concentrations differ by less than half an order of magnitude for 10^{-18} bar, while a difference of 1-2 orders of magnitude was observed for 10^{-14} bar.

It should be noted that the present calculation of defect chemistry and space charge include an acceptor dopant. The present experiments used ceramic powder processed from high purity raw materials (>99.9% purity) and the overall impurity levels as measured by ICP-OES are very low [21]. The most important impurities are Zr from the milling process (~600µg/g) and Ba (~100µg/g) and Ca (250µg/g) both from the raw material. Zr and Ba are isovalent dopants for the perovskite, so that they do not impact the bulk defect chemistry. However, they could still segregate to the grain boundaries due to lattice strain effects. Ca can be an isovalent dopant on the A-site of the perovskite, but also an acceptor dopant on the B-site. There are additional trace elements in the raw materials and introduced during powder processing that act as aliovalent dopants. Overall, these dopant species result in a significant acceptor doping of nominally undoped strontium titanate [44]. To account for this effect, the simulations included an acceptor dopant concentration of 10^{19} cm^{-3}.

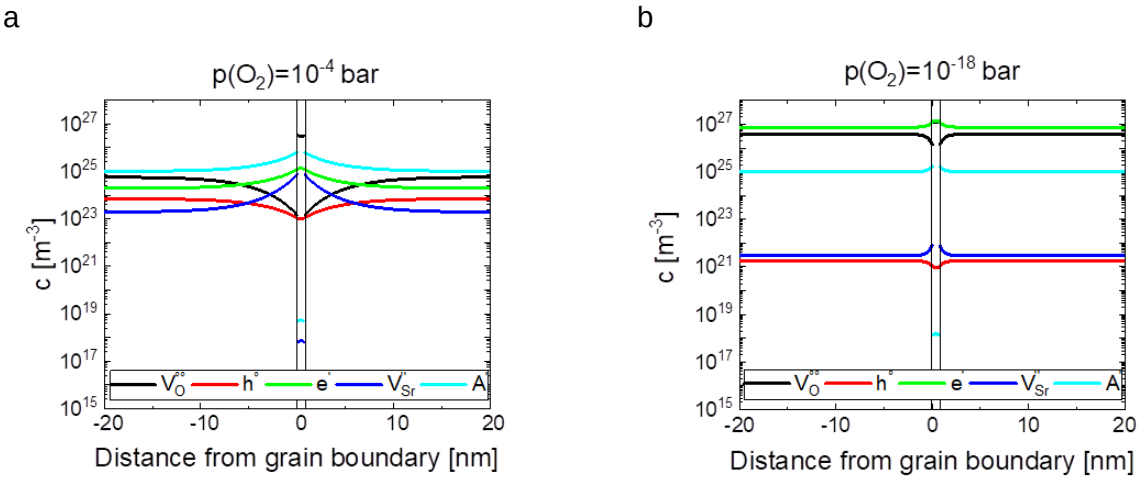

Figure 6 Defect distribution profiles for the grain boundary core and the space charge layer at 1400 °C for an oxygen partial pressure of 10^{-4} bar (a) and 10^{-18} bar (b). In both cases, the grain boundary core with its distinct defect concentrations is marked by vertical lines.

Accumulation (and depletion) of point defects on grain boundaries can impact grain boundary migration, if the respective defect has a relatively slow diffusion coefficient [22, 28]. To understand this effect, first grain growth without defect accumulation at the grain boundaries should be considered: In this case, an interface migrates by atoms breaking their bonds to the shrinking lattice and forming new bonds to the growing lattice. This process seems not to involve diffusion over a range much longer than one unit cell.

If now defect accumulation is added to the boundaries, the accumulated species in the space charge will need to diffuse together with the migrating boundary. As the space charge layer extends over much more than one unit cell, a significant diffusion of the accumulated (or depleted) defects is now implied. Therefore, grain boundary migration will experience a diffusional drag and the space charge layer will become asymmetric as sketched in Figure 7b. This argumentation is analogue to the theory of solute drag, which was established for grain boundary migration in metals with segregating solutes [45, 46].

Figure 6a and b showed the change of the defect accumulation with oxygen partial pressure (almost no defect accumulation and space charge for 10^{-18} bar in b and strong defect accumulation for 10^{-4} bar in a). Based on these defect profiles, it seems to be likely that for high oxygen partial pressure a diffusional drag arises from the accumulation of acceptors and/or strontium vacancies (Figure 7a), while for low oxygen partial pressure and no accumulation a diffusional drag is not expected (Figure 7b). Accordingly, slow (fast) grain boundary migration and mobility are expected for high (low) oxygen partial pressure and low (high) oxygen vacancy concentration.

However, this entire framework only holds if there are slowly diffusing species in the space charge layer that follow grain boundary migration. As electrons, holes and oxygen vacancies

can be assumed to have a high diffusion coefficient in strontium titanate [32], the relevant species for the diffusional drag are acceptors and strontium vacancies. The diffusion of Sr vacancies is in the order of 10^{-20} to 10^{-14} cm²/s at 1400 °C [35, 36, 47-49] (oxygen vacancy diffusion is in the order of 10^{-5} cm²/s at 1400 °C [32]). To our best knowledge there is no diffusion data for dopants in strontium titanate, but as they occupy cation lattice cites, their diffusion will most probably not be faster than the respective metal vacancy and the diffusion coefficients for Sr vacancies represents a reasonable maximum for the dopant diffusion coefficient. Accordingly, the slowly diffusing species required for a diffusional drag on grain boundary motion are present (Sr vacancies and impurities), although it is not clear if only the acceptors or additionally the Sr vacancies are involved. However, the discussed mechanism agrees well with the experimental findings for grain growth in the absence of electric field, but with a change of $p(O_2)$. Faster grain growth and higher grain boundary mobilities where found, if grain growth occurred in forming gas (95% N_2 and 5% H_2) [30] compared to grain growth in oxygen [22, 23, 28, 50]. It also agrees well with the experimental findings on grain growth in electric field in strontium and barium titanate [18, 20].

To further detail the proposed mechanism of a diffusional drag, a detailed study of diffusion kinetics and grain boundary migration is needed. An import question is whether the cation defects (both intrinsic and extrinsic) are able to follow grain boundary migration. Their diffusion could either be too fast to have a significant impact on grain boundary migration or too slow to follow grain boundary migration at all. If no or not all cation defects are able to follow the grain boundary migration, the boundary chemistry will be changed to a non-equilibrium state and the grain boundary potential and space charge will be changed. In this regard, the present paper does only give a qualitative model for the dependence of grain boundary migration on space charge properties. A thermodynamically valid modelling using e.g. the phase field method is needed to account for the impact of grain boundary migration on space charge. On the other hand, high resolution TEM analysis of the grain boundary stoichiometry and chemistry with respect to $p(O_2)$ in field-free samples and with respect to position for samples in electric field could shed light on the occurring space charge and defect accumulation during grain growth.

Finally, it should be noted that the acceptor dopant concentration for the defect chemical calculations was assumed to be $10^{19} cm^{-3}$. This concentration is rather high and there is no direct evidence for this specific concentration. In general, a different acceptor dopant concentration might alter the grain boundary potential in Figure 5 and the concentration profile of acceptors in Figure 6 would be changed [27]. However, the argumentation above is only qualitatively and would not change significantly if the acceptor dopant concentration would be slightly different.

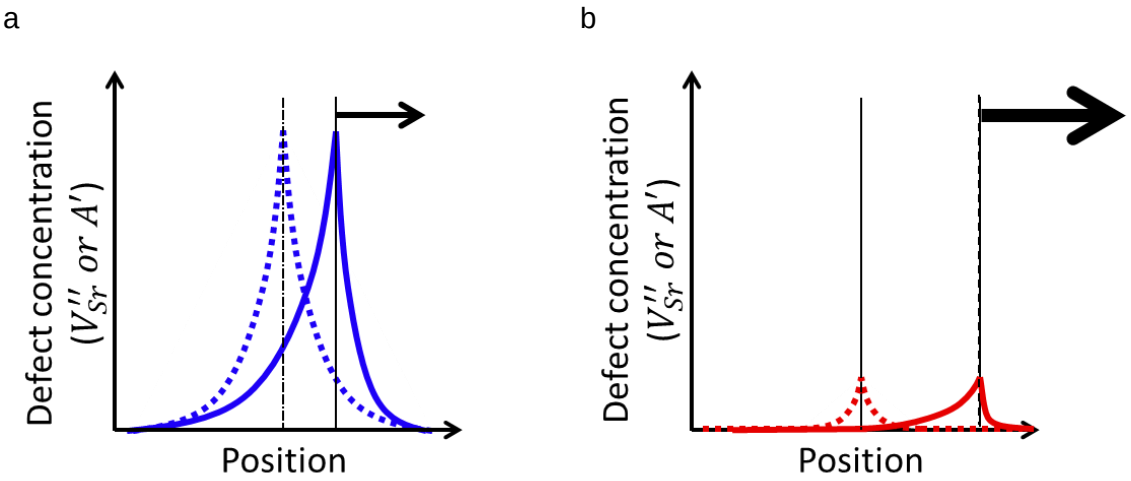

Figure 7 Impact of grain boundary migration on the space charge layers for strong (a) and weak (b) space charge as obtained for high (Figure 6a) and low (Figure 6b) oxygen partial pressure. The broken lines sketch the space charge layer without grain boundary migration. As less segregated point defects diffuse along with the grain boundary, faster grain boundary migration (i.e. higher grain boundary mobility) is expected for b.

3.4. ***What is the role of diffusion kinetics?***

The proposed mechanism for the formation of a gradient in the microstructure during grain growth in electric field is a diffusional drag by segregating defects at the grain boundaries and its change by the local defect chemistry. The entire argumentation bases on a defect redistribution of the oxygen vacancies across the entire sample by the electric field. Since this redistribution requires diffusion, kinetics become important for the defect concentration profile in the electric field. The experimental results at 1425 °C seem to indicate that diffusion kinetics could be limiting in this case as a gradient in the growth length of the single crystal was not visible for short heating times and low electric fields.

A very basic attempt to estimate the diffusion kinetics in the present experiment is assuming Browninan motion. As the electric field directs fluxes, the true diffusion kinetics will be faster and the following estimations will result in an overestimation of the equilibration time. Assuming a diffusion coefficient of 10^{-5} cm²/s at 1400 °C [32] and Brownian motion, a redistribution of the oxygen vacancies over the sample thickness of 2 mm would require about 0.5 h. However, at 1425 °C the gradient of the growth front of the single crystal was not visible after 10 h at 25 V/mm and not very pronounced at 50 V/mm (Figure 2). After 20 h, both fields resulted in a clear gradient. Again, assuming Brownian motion and a sample thickness of 2 mm, the diffusion coefficient would need to be as low as 10^{-7} cm²/s to give equilibration times of more than 10 h. The diffusion coefficient of 10^{-4} cm²/s was obtained for single crystals and diffusion in the polycrystal most likely is slower. However, the experimental setup contains a single

crystal and it is not clear why the diffusion coefficient of oxygen vacancies should be as low as 10^{-7} cm²/s for the present setup. On the other hand, the diffusion coefficient of strontium vacancies is still several orders of magnitude lower, so that its redistribution in electric field across the entire sample can be neglected at 1400 °C.

At 1550 °C, the oxygen vacancy diffusion coefficient is in the order of $3 \cdot 10^{-4}$ cm²/s and the estimated equilibration time is less than 1 min. This seems to be in good agreement with the experimental findings, where even for 6 min a pronounced gradient of grain growth was observed.

Clearly these estimations contain a significant error, since the diffusion is not by Brownian motion, but driven by an electric field. Accordingly, the true diffusion will be faster (and the equilibration times shorter) than estimated in this section. Nevertheless, we can conclude that strontium vacancies are most likely not involved in the long range defect redistribution across the entire sample. We can also conclude that at 1425 °C, some kinetic limitation seems to exist in the experiment, although it is not clear which process is kinetically limited (grain growth or the long-range diffusion of point defects). At 1550 °C kinetic limitations are unlikely to exist due to the fast diffusion of the oxygen vacancies at that temperature.

More detailed modelling of a defect redistribution in electric field can be found in the literature for titania [51] and strontium titanate [41]. However, these simulations considered much lower temperatures (900 °C for $SrTiO_3$), so that the results are not quantitatively applicable for the current case.

4. Summary and Conclusion

The present study observed grain growth of strontium titanate in electric field and attributes the observed effects to a point defect redistribution causing a change of space charge, defect accumulation and thereby diffusion and grain boundary mobility.

To observe grain growth in electric field, the seeded polycrystal technique was used where a single crystalline seed is diffusion-bonded to a polycrystalline matrix. The latter provides a well-controlled driving force for growth of the single crystal. The electric field was applied along the interface of the single crystal. Blocking electrodes where used to prevent a current flow and joule heating. During grain growth at 1425 °C and 1550 °C, the growth of the single crystal was faster at the negative electrode. At 1550 °C, this effect was visible for all fields and heating times. At 1425 °C, either higher field (50 V/mm) or long heating time (20 h) where needed to find significantly faster growth at the negative electrode.

The higher grain boundary mobility at the negative electrode was attributed to a defect redistribution of point defects in the electric field. An estimation of diffusion kinetics revealed that the only species that can redistribute during the experiments are the oxygen vacancies. A

thermodynamic calculation of the grain boundary potential and space charge showed that for high oxygen partial pressure (i.e. low oxygen vacancy concentration $[V_O^{\circ\circ}]$) a pronounced accumulation of intrinsic and extrinsic defects is present at the grain boundaries, while for low oxygen partial pressure (i.e. high $[V_O^{\circ\circ}]$) almost no accumulation of point defects occurs. As for grain boundary migration the segregated species diffuse along with the boundary, grain boundary migration with high $[V_O^{\circ\circ}]$ is expected to be faster than with low $[V_O^{\circ\circ}]$. As $\left[V_O^{\circ\circ}\right]$ is expected to be higher at the negative electrode, faster growth should occur there as found in the experiments.

The results suggest that the impact of space charge is an important parameter to understand microstructure evolution in ionic materials. The presented effect should occur in microstructure evolution in electric field if the following conditions are fulfilled:

1.) Presence of a charged point defect with high diffusivity
2.) Presence of space charge and accumulation of point defects with low diffusivity at the grain boundary (e.g. impurities)
3.) Dependence of space charge and defect accumulation on the defect chemistry

Gradients in the microstructure where observed for grain growth in electric field in other materials as barium titanate [18, 19] and zirconia [52] and in other field assisted processing techniques as SPS [5] and flash sintering [11]. These gradients could stem from a similar mechanism.

Finally, the observations shed new light on the understanding of grain growth in perovskite materials in the absence of electric fields. For both barium and strontium titanate it is well known that grain growth is faster in reducing atmosphere [30, 53, 54]. Based on the present findings, the link between the atmosphere and grain growth seems to be related to space charge and defect accumulation and its change with the defect chemistry. Space charge might also be important for the grain growth transition of strontium titanate, where the grain growth rate decreases with increasing temperature in a narrow temperature range of 1350 °C to 1425 °C [23].

Acknowledgement

A part of the work at KIT was supported by the German Research Foundation (DFG) under grant no. HO 1165/20-1 and SO 499/9-1 within the priority programme SPP1959.

References

[1] R. K. Bordia, S.-J. L. Kang, and E. A. Olevsky, “Current understanding and future research directions at the onset of the next century of sintering science and technology,” *Journal of the American Ceramic Society*, 2017.

[2] U. Anselmi-Tamburini, J. E. Garay, and Z. A. Munir, “Fundamental investigations on the spark plasma sintering/synthesis process iii. current effect on reactivity,” *Materials Science and Engineering A-structural Materials Properties Microstructure and Processing*, vol. 407, pp. 24–30, Oct. 2005.

[3] W. Chen, U. Anselmi-Tamburini, J. E. Garay, J. R. Groza, and Z. A. Munir, “Fundamental investigations on the spark plasma sintering/synthesis process - i. effect of dc pulsing on reactivity,” *Materials Science and Engineering A-structural Materials Properties Microstructure and Processing*, vol. 394, pp. 132–138, Mar. 2005.

[4] E. A. Olevsky and L. Froyen, “Impact of thermal diffusion on densification during sps,” *J. Am. Ceram. Soc.*, vol. 92, pp. S122–S132, JAN 2009.

[5] U. Anselmi-Tamburini, S. Gennari, J. Garay, and Z. Munir, “Fundamental investigations on the spark plasma sintering/synthesis process: Ii. modeling of current and temperature distributions,” *Materials Science and Engineering: A*, vol. 394, no. 1, pp. 139 – 148, 2005.

[6] M. Cologna, B. Rashkova, and R. Raj, “Flash sintering of nanograin zirconia in < 5 s at 850 degrees C,” *J. Am. Ceram. Soc.*, vol. 93, pp. 3556–3559, Nov. 2010.

[7] J. S. C. Francis, M. Cologna, and R. Raj, “Particle size effects in flash sintering,” *J. Eur. Ceram. Soc.*, vol. 32, pp. 3129–3136, Sept. 2012.

[8] M. C. Steil, D. Marinha, Y. Aman, J. R. C. Gomes, and M. Kleitz, “From conventional ac flash-sintering of YSZ to hyper-flash and double flash,” *J. Eur. Ceram. Soc.*, vol. 33, pp. 2093–2101, Oct. 2013.

[9] R. Baraki, S. Schwarz, and O. Guillon, “Effect of electrical field/current on sintering of fully stabilized zirconia,” *J. Am. Ceram. Soc.*, vol. 95, pp. 75–78, JAN 2012.

[10] K. Terauds, J. M. Lebrun, H. H. Lee, T. Y. Jeon, S. H. Lee, J. H. Je, and R. Raj, “Electroluminescence and the measurement of temperature during stage iii of flash sintering experiments,” *Journal of the European Ceramic Society*, vol. 35, pp. 3195–3199, Oct. 2015.

[11] M. Yu, S. Grasso, R. Mckinnon, T. Saunders, and M. J. Reece, “Review of flash sintering: materials, mechanisms and modelling,” *Advances In Applied Ceramics*, vol. 116, no. 1, pp. 24–60, 2017.

[12] J. Narayan, “A new mechanism for field-assisted processing and flash sintering of materials,” *Scr. Mater.*, vol. 69, pp. 107–111, July 2013.

[13] G. CORAPCIOGLU, M. A. Gülgün, K. KISSLINGER, S. STURM, S. JHA, and R. RAJ, “Microstructure and microchemistry of flash sintered $K_{0.5}Na_{0.5}NbO_3$,” *Journal of the Ceramic Society of Japan*, vol. 124, pp. 321–328, 2016.

[14] R. I. Todd, E. Zapata-Solvas, R. S. Bonilla, T. Sneddon, and P. R. Wilshaw, “Electrical characteristics of flash sintering: thermal runaway of joule heating,” *Journal of the European Ceramic Society*, vol. 35, pp. 1865–1877, June 2015.

[15] W. Ji, B. Parker, S. Falco, J. Y. Zhang, Z. Y. Fu, and R. I. Todd, “Ultra-fast firing: Effect of heating rate on sintering of 3YSZ, with and without an electric field,” *Journal of the European Ceramic Society*, vol. 37, pp. 2547–2551, June 2017.

[16] F. Lemke, W. Rheinheimer, and M. J. Hoffmann, “A comparison of power controlled flash sintering and conventional sintering of strontium titanate,” *Scripta Materialia*, vol. 130, pp. 187–190, 2017.

[17] H. Majidi, T. B. Holland, and K. van Benthem, “Quantitative analysis for in situ sintering of 3% yttria-stablized zirconia in the transmission electron microscope,” *Ultramicroscopy*, vol. 152, pp. 35–43, Mar. 2015.

[18] H. R. Jin, S. H. Yoon, J. H. Lee, J. H. Lee, N. M. Hwang, D. Y. Kim, and J. H. Han, “Effect of external electric field on the grain-growth behavior of barium titanate,” *J. Am. Ceram. Soc.*, vol. 87, pp. 1747–1752, Sept. 2004.

[19] H. R. Jin, S. H. Yoon, J. H. Lee, N. M. Hwang, D. Y. Kim, and J. H. Han, “Effect of external electric field on the grain growth of barium titanate in N_2 atmosphere,” *Journal of Materials Science-materials In Electronics*, vol. 16, pp. 749–752, Nov. 2005.

[20] W. Rheinheimer, M. Fülling, and M. J. Hoffmann, “Grain growth in weak electric fields in strontium titanate: Grain growth acceleration by defect redistribution,” *J. Eur. Ceram. Soc.*, vol. 36, no. 11, pp. 2773 – 2780, 2016.

[21] M. Bäurer, H. Kungl, and M. J. Hoffmann, “Influence of Sr/Ti stoichiometry on the densification behavior of strontium titanate,” *J. Am. Ceram. Soc.*, vol. 92, pp. 601–606, 2009.

[22] W. Rheinheimer and M. J. Hoffmann, “Grain growth in perovskites: What is the impact of boundary transitions?,” *Current Opinion in Solid State and Materials Science*, vol. 20, no. 5, pp. 286 – 298, 2016.

[23] W. Rheinheimer and M. J. Hoffmann, “Non-arrhenius behavior of grain growth in strontium titanate: New evidence for a structural transition of grain boundaries,” *Scr. Mater.*, vol. 101, pp. 68–71, May 2015.

[24] R. Moos and K. Härdtl, “Defect chemistry of donor-doped and undoped strontium titanate ceramics between 1000°C and 1400°C,” *J. Am. Ceram. Soc.*, vol. 80, no. 10, pp. 2549–2562, 1997.

[25] H. Sternlicht, W. Rheinheimer, M. J. Hoffmann, and W. D. Kaplan, “The mechanism of grain boundary motion in $SrtTO_3$,” *J. Mater. Sci.*, vol. 51, pp. 467–475, 2015.

[26] S. von Alfthan, N. A. Benedek, L. Chen, A. Chua, D. Cockayne, K. J. Dudeck, C. Elsaesser, M. W. Finnis, C. T. Koch, B. Rahmati, M. Rühle, S.-J. Shih, and A. P. Sutton, “The structure of grain boundaries in strontium titanate: Theory, simulation, and electron microscopy,” in *Annual Review of Materials Research* (D. Clarke, M. Ruhle, and F. Zok, eds.), vol. 40 of *Annual Review of Materials Research*, pp. 557–599, 2010.

[27] R. A. De Souza, “The formation of equilibrium space-charge zones at grain boundaries in the perovskite oxide $SrTiO_3$,” *Physical Chemistry Chemical Physics*, vol. 11, no. 43, pp. 9939–9969, 2009.

[28] W. Rheinheimer, M. Bäurer, C. Handwerker, J. Blendell, and M. Hoffmann, “Growth of single crystalline seeds into polycrystalline strontium titanate: Anisotropy of the mobility, intrinsic drag effects and kinetic shape of grain boundaries,” *Acta Materialia*, vol. 95, no. 0, pp. 111 – 123, 2015.

[29] W. Rheinheimer, M. Bäurer, H. Chien, G. S. Rohrer, C. A. Handwerker, J. E. Blendell, and M. J. Hoffmann, “The equilibrium crystal shape of strontium titanate and its relationship to the grain boundary plane distribution,” *Acta Mat.*, vol. 82, pp. 32–40, 2015.

[30] W. Rheinheimer, M. Bäurer, and M. Hoffmann, “A reversible wetting transition in strontium titanate and its influence on grain growth and the grain boundary mobility,” *Acta Mater.*, vol. 101, pp. 80–89, 05 2015.

[31] R. A. De Souza, J. Fleig, R. Merkle, and J. Maier, “$SrTiO_3$: a model electroceramic,” *Z. Metallkd.*, vol. 94, no. 3, pp. 218–225, 2003.

[32] R. A. De Souza, “Oxygen diffusion in $SrTiO_3$ and related perovskite oxides,” *Advanced Functional Materials*, vol. 25, pp. 6326–6342, Oct. 2015.

[33] T. Shi, Y. Chen, and X. Guo, “Defect chemistry of alkaline earth metal (Sr/Ba) titanates,” *Progress in Materials Science*, vol. 80, pp. 77 – 132, 2016.

[34] R. A. De Souza, Z. A. Munir, S. Kim, and M. Martin, “Defect chemistry of grain boundaries in proton-conducting solid oxides,” *Solid State Ionics*, vol. 196, pp. 1–8, Aug. 2011.

[35] R. Meyer, R. Waser, J. Helmbold, and G. Borchardt, “Cationic surface segregation in donor-doped $SrTiO_3$ under oxidizing conditions,” *JOURNAL OF ELECTROCERAMICS*, vol. 9, pp. 103–112, NOV 2002.

[36] R. Meyer, R. Waser, J. Helmbold, and G. Borchardt, “Observation of vacancy defect migration in the cation sublattice of complex oxides by ^{18}O tracer experiments,” *Phys. Rev. Lett.*, vol. 90, no. 10, p. 105901, 2003.

[37] R. Waser, T. Baiatu, and K.-H. Härdtl, “dc electrical degradation of perovskite-type titanates: I, ceramics,” *J. Am. Ceram. Soc.*, vol. 73, no. 6, pp. 1645–1653, 1990.

[38] R. Waser, T. Baiatu, and K.-H. Härdtl, “dc electrical degradation of perovskite-type titanates: Ii, single crystals,” *J. Am. Ceram. Soc.*, vol. 73, no. 6, pp. 1654–1662, 1990.

[39] R. Waser, T. Baiatu, and K.-H. Härdtl, “dc electrical degradation of perovskite-type titanates: Iii, a model of the mechanism,” *J. Am. Ceram. Soc.*, vol. 73, no. 6, pp. 1663–1673, 1990.

[40] R. Meyer, R. Liedtke, and R. Waser, “Oxygen vacancy migration and time-dependent leakage current behavior of $Ba_{0.3}Sr_{0.7}TiO_3$ thin films,” *Appl. Phys. Lett.*, vol. 86, pp. 112904/1–3, 2005.

[41] J. J. Wang, H. B. Huang, T. J. M. Bayer, A. Moballegh, Y. Cao, A. Klein, E. C. Dickey, D. L. Irving, C. A. Randall, and L. Q. Chen, “Defect chemistry and resistance degradation in Fe-doped $SrTiO_3$ single crystal,” *Acta Materialia*, vol. 108, pp. 229–240, Apr. 2016.

[42] Y.-M. Chiang and T. Takagi, “Grain-boundary chemistry of barium titanate and strontium titanate: I, high-temperature equilibrium space charge,” *J. Am. Ceram. Soc.*, vol. 73, no. 11, pp. 3278–3285, 1990.

[43] Y.-M. Chiang and T. Takagi, “Grain-boundary chemistry of barium titanate and strontium titanate: Ii, origin of electrical barriers in positive-temperature-coefficient thermistors,” *J. Am. Ceram. Soc.*, vol. 73, pp. 3286–3291, 1990.

[44] N.-H. Chan, R. Sharma, and D.M.Smyth, “Nonstoichiometry in $SrTiO_3$,” *Japan Elektrochemical Society*, vol. 128, no. 8, pp. 1762–1769, 1981.

[45] J. W. Cahn, “Impurity-drag effect in grain boundary motion,” *Acta Metallurgica*, vol. 10, p. 789, 1962.

[46] K. Lücke and K. Detert, “A quantitative theory of grain-boundary motion and recrystallization in metals in the presence of impurities,” *Acta Metallurgica*, vol. 5, no. 11, pp. 628–637, 1957.

[47] F. Lemke, W. Rheinheimer, and M. Hoffmann, “Sintering and grain growth in $SrTiO_3$: impact of defects on kinetics,” *Journal of Ceramic Society of Japan*, vol. 124, no. 4, pp. 346–353, 2016.

[48] K. Gömann, G. Borchardt, M. Schulz, A. Gömann, W. Maus-Friedrichs, B. Lesage, O. Kaitasov, S. Hoffmann-Eifert, and T. Schneller, “Sr diffusion in undoped and La-doped $SrTiO_3$ single crystals under oxidizing conditions,” *Phys. Chem. Chem. Phys.*, vol. 7, pp. 2053 – 2060, 2005.

[49] E. P. BUTLER, H. JAIN, and D. M. SMYTH, “Cation interdiffusion in polycrystalline calcium and strontium-titanate,” *Journal of the American Ceramic Society*, vol. 74, pp. 772–776, Apr. 1991.

[50] W. Rheinheimer and M. Hoffmann, “Grain growth transitions of perovskite ceramics and their relationship to abnormal grain growth and bimodal microstructures,” *Journal of Materials Science*, vol. HTC 2015, pp. 1–10, 2015.

[51] A. Moballegh and E. C. Dickey, “Electric-field-induced point defect redistribution in single-crystal TiO_{2-x} and effects on electrical transport,” *Acta Materialia*, vol. 86, pp. 352–360, Mar. 2015.

[52] Y. Dong, *Cation Kinetics And Electric Field Effect In Zirconia*. PhD thesis, University of Pennsylvania, 2017.

[53] S.-M. An and S.-J. L. Kang, “Boundary structural transition and grain growth behavior in $BaTiO_3$with Nd_2O_3 doping and oxygen partial pressure change,” *Acta Mater.*, vol. 59, no. 5, pp. 1964–1973, 2011.

[54] S.-Y. Chung, D. Y. Yoon, and S.-J. L. Kang, “Effects of donor concentration and oxygen partial pressure on interface morphology and grain growth behavior in $SrTiO_3$,” *Acta Mater.*, vol. 50, pp. 3361–3371, 2002.